

Fresnel filtering of Gaussian beams in microcavities

Susumu Shinohara,^{1,*} Takahisa Harayama,² and Takehiro Fukushima³

¹Max-Planck-Institut für Physik Komplexer Systeme, Nöthnitzer Straße 38, D-01187 Dresden, Germany

²NTT Communication Science Laboratories, NTT Corporation, 2-4 Hikaridai, Seika-cho, Soraku-gun, Kyoto 619-0237, Japan

³Department of Communication Engineering, Okayama Prefectural University, 111 Kuboki, Soja, Okayama 719-1197, Japan

*Corresponding author: susumu@pks.mpg.de

Compiled November 19, 2018

We study the output from the modes described by the superposition of Gaussian beams confined in the quasi-stadium microcavities. We experimentally observe the deviation from Snell's law in the output when the incident angle of the Gaussian beam at the cavity interface is near the critical angle for total internal reflection, providing direct experimental evidence on the Fresnel filtering. The theory of the Fresnel filtering for a planar interface qualitatively reproduces experimental data, and a discussion is given on small deviation between the measured data and the theory.

© 2018 Optical Society of America

OCIS codes: 140.2020, 140.3410, 140.4780, 230.3990, 230.5750.

When a beam with finite angular spreads is incident to a dielectric interface with incident angle near the critical angle for total internal reflection, it is theoretically shown that its refracted beam exhibits deviation from Snell's law [1, 2]. Because of the dependence of Fresnel reflection on incident angle, some angular components are totally internally reflected, while others far from the critical incident angle are refracted out, resulting in an angular shift in the far-field emission pattern. This effect, named the Fresnel filtering (FF) [1, 2], implies the correction of ray optics in addition to the Goos-Hänchen effect [3] and has recently attracted attention in interpreting emission patterns from microcavities [4–9].

In experiments on GaN microlasers with quadrupolar deformed cavities [4], emission patterns were explained by the FF effect on the output from “scarred modes”, which are associated with the unstable periodic ray orbit. In case of the scarred modes, however, general properties on the mode profile are not well understood, making it difficult to quantitatively estimate the FF effect. Considering that the original theory was established for Gaussian beams [1, 2], it is desirable to experimentally study the FF effect for the modes that are well described by the superposition of Gaussian beams. In this Letter, we study such modes for the quasi-stadium cavities, where Gaussian mode characteristics can be estimated by the Gaussian-optic theory [10]. We experimentally demonstrate the deviation from Snell's law and provide an analysis based on the FF theory.

Figure 1 (a) shows the geometry of the quasi-stadium cavity [11]. In this Letter, we study microlasers with quasi-stadium shape with cavity widths $W=100 \mu\text{m}$, $150 \mu\text{m}$, $190 \mu\text{m}$, and $200 \mu\text{m}$, while we fix the cavity length $L=600 \mu\text{m}$. The radius R of curvature of both curved edges is fixed as $R=L$ (i.e., confocal resonator condition). The devices are fabricated by using a MOCVD-grown gradient-index, separate-confinement-heterostructure, single-quantum-

well GaAs/ $\text{Al}_x\text{Ga}_{1-x}\text{As}$ structure and a reactive-ion-etching technique [11].

The confocal resonator condition yields that the Fabry-Perot orbit (bouncing between the boundary points A and C) and the ring orbit (reflected at A, B, C, and D) are both stable. In previous studies of the quasi-stadium microlasers, selective excitation of the Fabry-Perot modes and that of the ring modes were studied in detail [11]. The selective excitation has been successfully demonstrated by patterning the “contact window”, where electric currents are injected, along the Fabry-Perot orbit or the ring orbit. In this Letter, we consider the devices with the contact window patterned along the ring orbit with $5 \mu\text{m}$ width (see Ref. [11] for the details on the device structure and fabrication process) and study

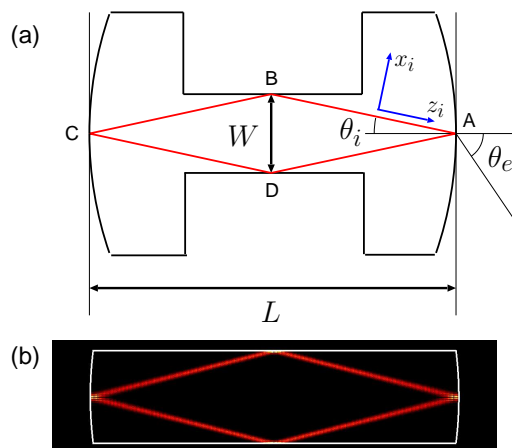


Fig. 1. (Color online) (a) The geometry of the quasi-stadium cavity with $L = 600 \mu\text{m}$ and $W = 150 \mu\text{m}$. The radius R of curvature of both curved edges is $600 \mu\text{m}$. Inside the cavity, the ring orbit reflected at the boundary points A, B, C, and D is shown. (b) Resonant mode associated with the ring orbit with the wavelength $\lambda \approx 0.856 \mu\text{m}$ calculated by the Gaussian-optic theory.

output from the ring modes as depicted in Fig. 1 (b).

In the ray-optic limit, the output can be predicted by Snell's law. We denote θ_i and θ_e the incident and the refracted angle, respectively, as illustrated in Fig. 1 (a). For given L and W , the incident angle is given by

$$\theta_i = \sin^{-1} \left(\frac{W}{\sqrt{L^2 + W^2}} \right). \quad (1)$$

Snell's law implies the refracted angle $\theta_e = \sin^{-1}(n \sin \theta_i)$, where n is the effective refractive index of the cavity, calculated as 3.3 from the structure of the devices. The ring orbit is confined by total internal reflection when the incident angle is above the critical angle $\theta_c = \sin^{-1}(1/n) \approx 17.64^\circ$. In terms of the cavity geometry, total internal reflection of the ring orbit occurs for $W > L/\sqrt{n^2 - 1} \approx 191 \mu\text{m}$. Below we compare experimentally measured emission patterns with the predictions by Snell's law.

In experiments, devices are tested at 25°C using a pulsed current with 500 ns width at 1 kHz repetition. The strength of an injection current is determined so that the peak output power exceeds 5 mW. Measured far-field patterns for the devices with various cavity widths are shown in Fig. 2 (solid curves). The definition of the far-field angle ϕ is given in Fig. 2 (d). The patterns are normalized so that the maximum intensity becomes unity. We indicate the prediction from Snell's law by vertical lines.

For $W = 100 \mu\text{m}$ (i.e., $\Delta\theta = \theta_c - \theta_i \approx 8.2^\circ$) and $W = 150 \mu\text{m}$ (i.e., $\Delta\theta \approx 3.6^\circ$), we find that the output peaks are in good agreement with the predictions from Snell's law. This agreement convinces us the validity of our estimate of the effective refractive index $n = 3.3$. For $W = 190 \mu\text{m}$ (i.e., $\Delta\theta \approx 0.068^\circ$), however, we see apparent deviation of the experimental data from Snell's law. More strikingly, for $W = 200 \mu\text{m}$ (i.e., $\Delta\theta \approx -0.80^\circ$), Snell's law predicts total internal reflection, but the experimental data show the output peaks around $\phi = \pm 77^\circ$.

The observed phenomenon is theoretically understood by the FF effect. Here, we present an analysis based on the theory by Tureci and Stone [1, 2]. First, we assume that the modes associated with the ring orbit are well described as the superposition of Gaussian beams. This is, in fact, justified by the Gaussian-optic theory in the short-wavelength limit [10]. As the sizes of our cavities are quite large compared to the wavelength (i.e., $nkR \approx 10^4$), the above assumption is well satisfied. Below, we focus on the Gaussian beam

$$E_i(x_i, z_i) = \frac{E_0 w_0}{w(z_i)} \exp \left[- \left(\frac{x_i}{w(z_i)} \right)^2 + inkz_i \right], \quad (2)$$

with $w^2(z_i) = w_0^2 - i(2z_i)/(nk)$ scattered at the boundary point A. The definition of the coordinates (x_i, z_i) is given in Fig. 1 (a). The beam waist w_0 , the distance between the beam waist position and the interface z_0 , and wavenumber k can be estimated by applying the

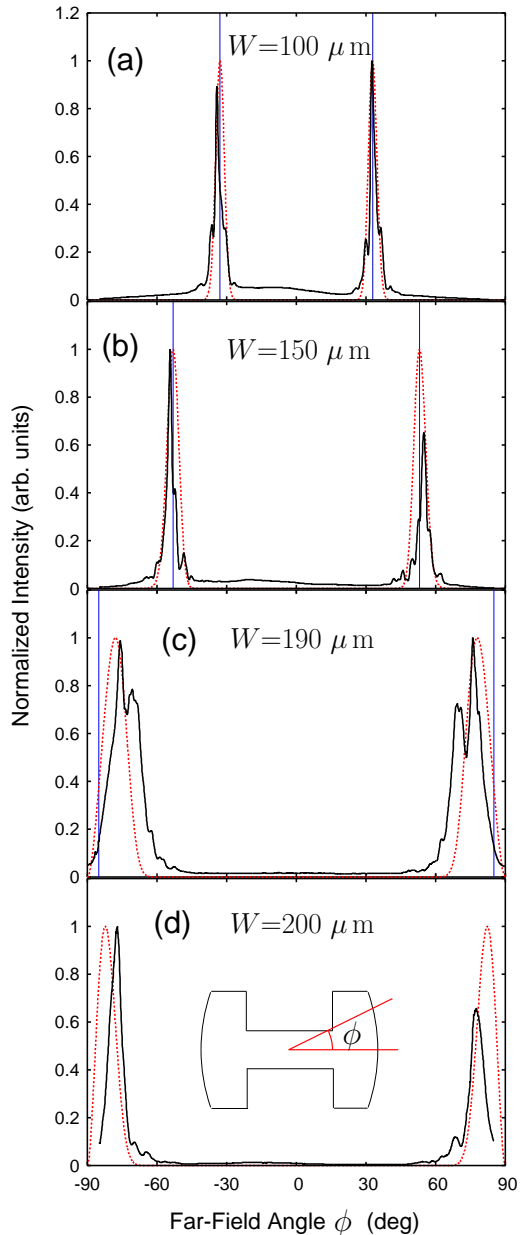


Fig. 2. (Color online) Far-field emission patterns of the quasi-stadium microlasers with (a) $W=100 \mu\text{m}$, (b) $W=150 \mu\text{m}$, (c) $W=190 \mu\text{m}$, and (d) $W=200 \mu\text{m}$. The definition of the far-field angle ϕ is given in the inset of (d). Experimental data are plotted with solid curves, while the predictions by the FF theory in dotted curves. The predictions by Snell's law are indicated by vertical lines.

Gaussian-optic theory to the ring orbit. Letting $(\alpha, \beta)^T$ the eigenvector of the stability matrix for a segment of the ring orbit (see Ref. [10] for details), we can write $w_0 = 1/(\sqrt{nk}|\alpha|)$ and $z_0 = -\text{Re}(\alpha\beta^*)/|\alpha|^2$.

For a given W , we consider the ring mode with the wavelength $\lambda \approx 0.856 \mu\text{m}$, which corresponds to the lasing wavelength in the experiments. In order to simplify the calculation, we employ the Dirichlet boundary

condition, instead of the dielectric boundary condition. This approximation does not affect so much the modal structure inside the cavity when the wavelength is sufficiently short. The field intensity distribution of a calculated mode for $W = 150 \mu\text{m}$ is shown in Fig. 1 (b). From the Gaussian-optic calculation, we found that for the cavities with $W = 100 - 200 \mu\text{m}$, the Gaussian beam is characterized by $nk \approx 24 \mu\text{m}^{-1}$ and $w_0 \approx 5 \mu\text{m}$, and the beam waist is located at the boundary points B and D, i.e., $z_0 = \sqrt{L^2 + W^2}/2$.

Next, we consider how the Gaussian beam is refracted at the boundary point A. In the polar coordinates (ρ, ϕ) , the refracted electric field has the following asymptotic form in the limit $k\rho \rightarrow \infty$ [1, 2]:

$$E_e(\rho, \phi) \approx \frac{nk w_0 E_0}{\sqrt{2ik\rho}} t(s_0) G(s_0) J(\phi, s_0) e^{ik\rho}, \quad (3)$$

where $s_0 = s_0(\phi)$ is determined by solving the equation $n \sin(\theta_i + \delta\theta_i(s)) = \sin \phi$ in terms of s with $\delta\theta_i = \sin^{-1}(s)$. $t(s)$ is the Fresnel transmission coefficient for the transverse electric polarization, $G(s)$ carries the information on the incident Gaussian beam, and $J(\phi, s)$ arises from the stationary phase approximation in deriving Eq. (3). These functions are defined as follows:

$$t(s) = \frac{2n \cos(\Theta_i(s))}{\cos(\Theta_i(s)) + n^2 \sqrt{\sin^2 \theta_c - \sin^2(\Theta_i(s))}}, \quad (4)$$

$$G(s) = \exp \left[- \left(\frac{nk w_0}{2} \right)^2 s^2 + ink z_0 \sqrt{1 - s^2} \right], \quad (5)$$

$$J(\phi, s) = \frac{\cos \phi \sqrt{1 - s^2}}{\sqrt{n^2 - \sin^2 \phi}}, \quad (6)$$

where $\Theta_i(s) = \theta_i + \delta\theta_i(s)$. Using Eq. (3) with nk , w_0 , and z_0 estimated from the Gaussian-optic theory, we calculated theoretical far-field patterns, which are plotted with dotted curves in Fig. 2.

When the incident angle θ_i is far from the critical angle θ_c (i.e., for $W = 100 \mu\text{m}$ and $W = 150 \mu\text{m}$), we find that the peak positions of the theoretical curves coincide with the predictions by Snell's law. However, the FF effect appears when θ_i is near θ_c . For $W = 190 \mu\text{m}$, we find noticeable deviation between the peak positions of the theoretical curve and the prediction by Snell's law. Moreover, for $W = 200 \mu\text{m}$, where Snell's law predicts total internal reflection, we find the maxima of the theoretical curve around $\phi = \pm 82^\circ$.

When $\theta_i \ll \theta_c$, Eq. (3) predicts that the far-field peak position is almost constant with respect to a change of the beam waist w_0 , while the peak width varies. Fitting the experimental data for $W = 100 \mu\text{m}$ by Eq. (3) with w_0 being a free parameter, we found that the peak width is best reproduced with $w_0 \approx 5 \mu\text{m}$. This convinces us that our estimate of w_0 from the Gaussian-optic theory is reliable.

The theoretical curves qualitatively explain the shifts from Snell's law observed in the experimental data, but

they underestimate the sizes of the shifts. The deviation is 4.9° for $W = 190 \mu\text{m}$, while 5.0° for $W = 200 \mu\text{m}$, where for a double peak of $W = 190 \mu\text{m}$, we compared the average of the two peak positions with the peak position of the theoretical curve.

For $\theta_i \approx \theta_c$, Eq. (3) predicts that the far-field peak position starts to depend on the beam waist w_0 . This suggests a possibility that a slight error in estimating w_0 shifts the peak position of Eq. (3). For the experimental data for $W = 190 \mu\text{m}$ and $W = 200 \mu\text{m}$, we found that in order to explain the measured peak positions by Eq. (3), one needs to put $w_0 \approx 2.5 \mu\text{m}$, which deviates too much from the estimate from the Gaussian-optic theory. Hence, we conclude that the deviations between the FF theory and the experimental data cannot be solely attributed to errors in w_0 .

The FF theory assumes an infinite planar interface, whereas the actual interface has curvature. This can be another cause for the deviations, although currently we lack a theory that quantitatively predicts the effect of curvature. Equation (3) reproduces the experimental data very well when $\theta_i \ll \theta_c$ and its deviations from the experimental data are observed only when $\theta_i \approx \theta_c$. Therefore, we expect a mechanism making the curvature effect prominent especially when $\theta_i \approx \theta_c$.

S.S. acknowledges financial support from DFG research group 760 "Scattering Systems with Complex Dynamics" and the DFG Emmy Noether Program.

References

1. H. E. Tureci and A. D. Stone, *Opt. Lett.* **27**, 7 (2002).
2. H. E. Tureci, Ph. D thesis, Yale University, 2003.
3. F. Goos and H. Hänchen, *Ann. Physik* **436**, 333 (1947).
4. N. B. Rex, H. E. Tureci, H. G. L. Schwefel, R. K. Chang, and A. D. Stone, *Phys. Rev. Lett.* **88**, 094102 (2002).
5. S. -Y. Lee, S. Rim, J. -W. Ryu, T. -Y. Kwon, M. Choi, and C. -M. Kim, *Phys. Rev. Lett.* **93**, 164102 (2004).
6. H. Schomerus and M. Hentschel, *Phys. Rev. Lett.* **96**, 243903 (2006).
7. E. G. Altmann, G. Del Magno, and M. Hentschel, *Europhys. Lett.* **84**, 10008 (2008).
8. J. Unterhinninghofen and J. Wiersig, *Phys. Rev. E* **82**, 026202 (2010).
9. Q. H. Song, L. Ge, A. D. Stone, H. Cao, J. Wiersig, J. -B. Shim, J. Unterhinninghofen, W. Fang, and G. S. Solomon, *Phys. Rev. Lett.* **105**, 103902 (2010).
10. H. E. Tureci, H. G. L. Schwefel, A. D. Stone, and E. E. Narimanov, *Opt. Express* **10**, 752 (2002).
11. T. Fukushima and T. Harayama, *IEEE J. Sel. Top. Quantum Electron.* **10**, 1039 (2004).